Flow in Confined Geometry Introduced by Dewetting of Ultrathin Polystyrene Films

E. Bauer,[†] E. Maurer,[†] T. Mehaddene,[†] S. V. Roth,[‡] and P. Müller-Buschbaum*,[†]

Physik-Department, TU München, LS E13, James-Franck-Str. 1, 85747 Garching, Germany, and HASYLAB at DESY, Notkestr. 85, 22603 Hamburg, Germany

Received March 10, 2006; Revised Manuscript Received May 22, 2006

ABSTRACT: By making use of dewetting, the flow of polystyrene (PS) in confined geometry of ultrathin films is investigated as a function of the boundary conditions. Four different surface treatment procedures have been applied to silicon (Si) substrates to realize small changes of the oxide surfaces. Atomic force microscopy and surface-sensitive scattering experiments show a change in the mass transport of PS. A slowing down in comparison to the well-known slip and no-slip conditions is observed, except in the case of binodal dewetting mechanisms, which obeys a partial slippage. In addition to the changed kinetic behavior, the final states show big differences in the contact angle of the drops. Our results are explained within a model, which includes changes of the short-ranged part of the wall potential due to different oxide layer thicknesses, introduced by the treatment processes.

Introduction

In general, flow of a liquid upon a solid surface is controlled by interactions on different length scales: The interactions between the constituents of the liquid and the solid substrate on the atomic scale as well as the substrate morphology in terms of corrugation, roughness, and topography on a large length scale give rise to a rich system-specific behavior.

Microfluidic devices which manipulate microquantities of liquid solutions allow for substantial improvement of the efficiency of chemical processes. The exact control of mixing and separation processes during fluid flow in confined geometries is thereby essential for many applications as microanalytics or high-throughput devices and reactors[1−5] as well as for analytical applications, as in chromatography. For the design of new down-scaled microfluidic devices and lab-on-chip (LOC) systems the understanding of flow in confined geometry is essential. In an open geometry, the polymer chains are constrained on the substrate surface, thereby introducing a confinement.

Macroscopic flow on surfaces is easily realized by the presence of a source or drain of the liquid and forces such as gravity are well-suited to drive mass transport. For the observation of moving macroscopic liquid fronts optical techniques are readily used. However, to address flow on smaller scale, other concepts have to be applied.

For the identification of confinement effects nanoscopic flow was investigated. The handling of extremely tiny amounts of liquids on the order of sub-microliters turned out to force several changes in the experiments. On one hand, the resulting liquid droplets are on the order of 300 nm in diameter only, corresponding to a volume of 7 aL and thus no longer observable with optical techniques. As a consequence, atomic force microscopy (AFM) is used for the real-space investigation, accompanied by scattering experiments based on grazing incidence small-angle X-ray scattering (GISAXS).[11] On the other hand, such amounts of liquids are no longer reproducibly deposited, and the inspection of single droplets imposes large experimental errors. Moreover, by gravitation such as acting on an incline[12] no movement is obtained. Therefore, ensembles of tiny droplets are investigated, and the interaction with the underlying substrate is used as a driving force of the movement.

For this purpose, dewetting[14] of an initially homogeneous, continuous, and ultrathin but metastable film is utilized to study mass transport in the microscopic regime. The polymer film is not located between two (hard) walls, but between a solid support and air, thereby acting as a second wall. The impact of the boundary condition imposed by the substrate is addressed by four different substrate surface treatment procedures.[13] Slight modifications of the substrate result from these different treatments. As a consequence, this investigation pictures the sensitivity of flow in confined geometry on the actual surfaces present underneath the liquid. It will be of importance for a variety of tools for future microfluidics, as pumps,[6] valves,[6] channels,[7] and mixers[8−10] on the nanoscale.

The system under investigation, polystyrene (PS) on top of silicon (Si) covered with its oxide layer (SiOx), is among the most investigated model systems related to film instabilities (see for example refs 15−19). Its popularity arises from its apparent simplicity. Both major components, PS and Si, are commercially available with a high degree of purity and perfection. They are extensively characterized, and their relevant physical and chemical parameters are available in the literature.[20] With respect to the long-ranged part of the effective interface potential as long as only van der Waals contributions are taken into account, PS is stable on Si and unstable on SiOx. Thus, the oxide layer thickness enables a tuning of the film stability.[21]

Xie et al.[22] observed typical spinodal-like surface pattern evolve during further annealing in the case of 4K PS films with thicknesses below 10 nm on acid-cleaned Si. Because of the smaller molecular weight, these films were not that confined as compared to the ones presented in this investigation. In contrast, Seemann et al.[23] restricted the spinodal regime to a PS layer thickness below 2 nm in the case of a 1 nm oxide layer thickness. With increasing oxide layer thickness the value of the PS film thickness being unstable against spinodal dewetting increases in their investigation. However, because of the small molecular weight chosen (R_g = 1.2 nm for 2K) the confinement regime was not touched in the investigation of

[†] TU München.
[‡] HASYLAB at DESY.
* Corresponding author.

10.1021/ma060535y CCC: $33.50 © 2006 American Chemical Society
Published on Web 07/01/2006

Table 1. Values Obtained from the Fits to the Reflectivity Curves Measured at Samples after Different Si Surface Treatment, with Base, Acid, Milli-Q, and Wiping[a]

treatment	d_{PS} [nm]	d_{Ox} [nm]	σ [nm]
acid	6.2 ± 0.2	1.54 ± 0.10	0.72 ± 0.05
base	5.7 ± 0.1	1.35 ± 0.11	0.65 ± 0.05
Milli-Q	4.7 ± 0.1	1.20 ± 0.10	0.56 ± 0.06
wiping	6.2 ± 0.2	1.20 ± 0.12	0.67 ± 0.04

[a] PS film thickness $= d_{PS}$, oxide layer thickness $= d_{Ox}$, and surface roughness $= \sigma$.

Seemann et al.[23] Rehse et al.[24] observed an instability−stability transition of PS (molecular weights between 5.6K and 1000K) on corrugated as well as on flat Si substrates at a critical thickness. The critical thickness was reported to scale with the radius of gyration of the unperturbed chain. Films with thicknesses larger than $0.55R_g$ remained stable and ones with thicknesses smaller than $0.55R_g$ dewetted.[24]

Consequently, PS on Si appears to be well-suited for the investigation of flow phenomena. At first sight, it is even simpler than systems that require the deposition of an additional layer.[25] To investigate the sensitivity of the kinetics, four different surface treatment procedures have been applied to Si. As we will demonstrate, these different procedures only slightly affect the SiOx but largely alter the film stability and thereby the mass transport. In earlier work[13] the dramatic effect of a variation in the cleaning protocol was demonstrated for the system PS on Si covered with its native oxide. It was shown that in the case of thin and unconfined PS films different cleanings result in a film stability or a dewetting by nucleation and growth. Moreover, for ultrathin and confined PS films the lower limit of the film thickness of homogeneous films installable by spin-coating was determined.[13] Within this investigation we chose a thickness value which is well above this limit.

Flow of the polymer material is achieved by heating above the glass transition temperature of PS, thereby liquefying the polymer. Whereas thick PS films are stabilized by the long-ranged part of the effective interface potential, ultrathin films, with thickness comparable to the thickness of the oxide layer, are expected to be unstable. At the selected thickness of 5.7 ± 0.7 nm, which is ~4 times the oxide layer thickness, an intermediate regime is addressed.

After a short introduction into the experimental methods (atomic force microscopy, specular and off-specular X-ray scattering) the influence of the applied surface cleaning is addressed, and the resulting changes in the kinetic behavior are presented. A summary concludes the paper.

Experimental Section

Sample Preparation. Polystyrene (PS) with a molecular weight $M_w = 27\,500$ g/mol ($M_w/M_n = 1.04$) was spin-coated (2000 rpm, 30 s) from a toluene solution with concentration $c = 1.003$ mg/mL on top of differently cleaned native oxide-covered Si(100) surfaces (Wacker Siltronic, Burghausen). In total, prior to spin-coating four different cleaning processes were performed (see Table 1):[13] (1) The acid clean (denoted "acid") consists of 35 mL of deionized H_2O, 35 mL of H_2O_2, and 100 mL of H_2SO_4 heated to 80 °C for 15 min. Next, the substrates are flushed with water and dried with N_2. (2) For the base clean (denoted "base") the substrates are put in a dichloromethane bath for 30 min at 45 °C, followed by the storage in a base bath of 30 mL of NH_3, 30 mL of H_2O_2, and 350 mL of deionized water at 65 °C, which is heated to 75 °C. After 2 h at 75 °C the substrates are flushed with deionized water and dried with N_2. (3) 24 h storage in highly purified water and drying with N_2 define the third cleaning process (denoted "Milli-Q"). (4) A fourth surface treatment (denoted "wiping") consists of rubbing the silicon substrate surfaces with a toluene-soaked fuzz-free wipe (Kimwipe Lite, Kimberly-Clark). Several wiping in random direction are performed successively.

Within each cleaning series 8−10 individual samples were prepared to ensure reproducibility of the reported results. Given numbers are averaged, and the error bar gives an estimate of the deviation within one set of nominally identical samples.

After preparation of the initially homogeneous PS films upon the differently pretreated Si substrates, the samples were annealed. The annealing was performed on a heat plate in air, above the glass transition temperature of PS at 130 °C. The air provides good thermal contact and moreover might be more realistic with respect to possible microfluidic applications than vacuum conditions. Different annealing times were selected to focus on the early stages as well as on stability. After annealing the samples were quenched to room temperature and examined.

Atomic Force Microscopy. An Autoprobe CP (Vecco) atomic force microscope (AFM) was used for the investigation of the PS film surfaces. The operated gold-coated silicon cantilevers (Ultralever cantilevers) with a spring constant of $\cong 2.1$ N m^{-1} had a high aspect ratio. The tips had a typical radius of curvature of 10 nm, which is small as compared to the structures measured. All measurements were performed under air and at room temperature. The AFM height and lateral calibration was performed several times with calibration standards to improve the accuracy of the height and lateral information. Because of the hardware linearization of our AFM system, this calibration works over the covered range of heights and surface area. In the investigated confined ultrathin film thickness regime, the polymeric structures are highly sensitive, and only in the applied noncontact mode a tip-induced sample degradation is minimized. For each sample, micrographs at several different spatial positions of the surface were recorded with a scan range between 1 μm × 1 μm and 8 μm × 8 μm. From the raw data the background due to the scanner tube movement was fully subtracted.

Statistical information parallel to the surface was obtained by the calculation of the power spectral density function (PSD). It was calculated from the AFM pictures by a two-dimensional (2D) Fourier transformation and the radial average of the isotropic Fourier space data.[26] Because of the different scan ranges in real space, different intervals are covered in reciprocal space. So to cover a larger interval in reciprocal space, a merging of PSD curves related to different scan sizes was performed. These merged data are called a master curve and can directly be compared to a scattering signal. For example, the presence of peaks in the master curve denotes the existence of most prominent in-plane length scales in the resolvable range.[27]

X-ray Specular Scattering. X-ray reflectivity curves were measured with a laboratory Siemens D5000 diffractometer with a reflectivity extension. A knife edge was mounted above the sample surface to reduce background and control the footprint of the X-ray beam on the sample. The reflectivity measurements were performed at a wavelength of $\lambda = 0.154$ nm (secondary graphite monochromator, Cu Kα). Measurements were performed under air with a scintillation counter. A large q_z range was covered to allow for the detection of small changes in thickness of the thin films.

The fits to the reflectivity data were always performed with a model assuming a native oxide layer and a PS layer on top. Fitting was performed with the program Parratt3 (version 1.5.2),[28] yielding parameters such as film thicknesses and roughnesses. The samples were investigated directly after spin-coating of the PS layer (denoted with "as prepared").

X-ray Off-Specular Scattering. The sample surface is defined as the (x,y) plane. The incident beam is directed along the x-axis with an incident angle α_i. The (x,z) plane denotes the plane of incidence and reflection, and thus the condition for specular scattering is given by $q_x = q_y = 0$ and $q_z > 0$, with the scattering vector $\vec{q} = (q_x, q_y, q_z)$.[29] The specular peak fulfills the specular condition ($\alpha_i = \alpha_f$). Diffusely scattered intensity is observed for $q_x \neq 0$ or $q_y \neq 0$.

To probe lateral structures, grazing incidence small-angle X-ray scattering (GISAXS) was applied.[11,30,31] GISAXS is observed along the out-of plane direction and satisfies the condition $q_y \neq 0$. The

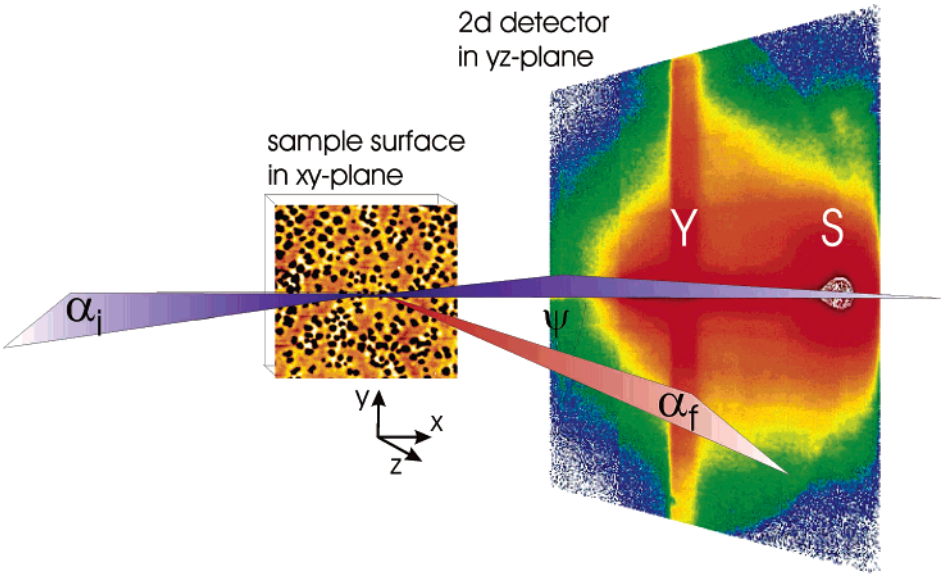

Figure 1. Schematic top view of the GISAXS geometry making use of a two-dimensional detector in the *yz* plane to picture the scattering geometry. The sample is placed in the *xy* plane. The incident angle is denoted α_i and the exit angle α_f. The structural information is obtained from a *y*-cut out of the two-dimensional intensity distribution perpendicular to the scattering plane (*xz* plane) indicated by the two opposite triangles. The GISAXS signal is probed as a function of the out-of-plane angle Ψ. As figuratively shown, the diffusely scattered intensity in the scattering plane exhibits a Yoneda peak (Y) and a specular peak (S) as common features.

GISAXS experiments were performed at the BW4 beamline at the synchrotron HASYLAB (DESY, Hamburg). The selected wavelength was $\lambda = 0.138$ nm. Details concerning the beamline are reported elsewhere.[32] The samples were placed horizontally on a two-circle goniometer with a *z*-translational table. A sample−detector distance of 12.56 m was selected to enable high resolution. A resolution better than 1.42×10^{-3} nm^{-1} was achieved. Consequently, the setup accessed lateral lengths from 35 nm up to 4400 nm. Nearly the full X-ray pathway was operated under ultrahigh-vacuum conditions. The beam quality was optimized by using a setup of high-quality entrance cross-slits. By using a 2D detector (Gabriel, 512 × 512 pixel array detector) the specular peak and the off-specular scattering were probed simultaneously. At one fixed angle of incidence $\alpha_i = 0.325°$ the 2D detector array can be understood as 512 vertical lines, representing so-called detector and off-detector scans,[29] or as 512 horizontal lines, GISAXS cuts.[11] Since an incident angle well above the critical angle of the materials under investigation (e.g., α_c(PS) = 0.138° and α_c(Si) = 0.200°) was chosen, the Yoneda peak and the specular peak are well separated on the 2D detector.[33,34]

A sketch of the typical setup along with the relevant angles is shown in Figure 1.

Results and Discussion

Initial Homogeneous PS Films. Directly after the Si substrates have been treated with one of the four surface cleaning procedures, a PS film is spin-coated on top. Spin-coating is well-suited to prepare homogeneous and continuous films.[35] These films can be meta- or unstable and dewet, if a mobility of the PS molecules is allowed. To probe the density profile perpendicular to the substrate surface of the as-prepared films and detect the parameters characterizing the oxide and PS layer, X-ray reflectivity has been applied. Representative data for each of the treatment series together with model fits are displayed in Figure 2. The small deviations between data and fit can be attributed to the restriction to a simple fitting model including only an oxide layer and a PS layer on top. As compared to the radius of gyration $R_g = 5.4$ nm of the used PS, the films under investigation are confined. Irrespective of the applied cleaning, the curves exhibit well-pronounced fringes in the intensity picturing the small interface and surface roughnesses of the

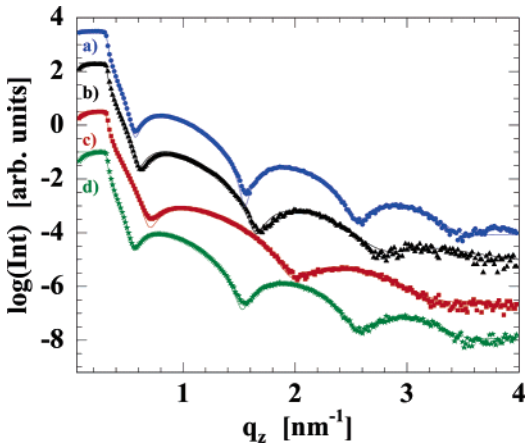

Figure 2. Reflectivity measurements (symbols) and fits to the experimental data (lines) of the as-prepared samples as a function of the wave vector component q_z. The different cleaning procedures are (a) base, (b) acid, (c) Milli-Q, and (d) wiping as explained in the Experimental Section. The curves are shifted along the *y*-axis for clarity.

oxide and PS. Different wavelengths of the intensity modulations between different cleaning series are obvious. Thus, the four types of films slightly differ in the initial PS film thickness (see Table 1). The given error bars include deviations between nominally identical samples prepared to test reproducibility as well as the errors from the model fit. Although spin-coating was applied with exactly identical conditions in terms of spinning parameters and polymer concentration of the solution used, the differences in the total PS thickness are on the order of 1 nm.

With respect to the commonly used spin-coating equation,[36] these differences, although small, are unexpected. Obviously, the applied surface treatment influences the surface chemistry of the Si substrates and thereby results in slightly changed conditions present in the spin-coating. Because of the very complicated nonlinear processes involved in spin-coating, a full theoretical understanding is still lacking.[37] In a simple model, the spin-coating process can be subdivided into three different stages:[38] First, a PS solution with a low concentration is dropped

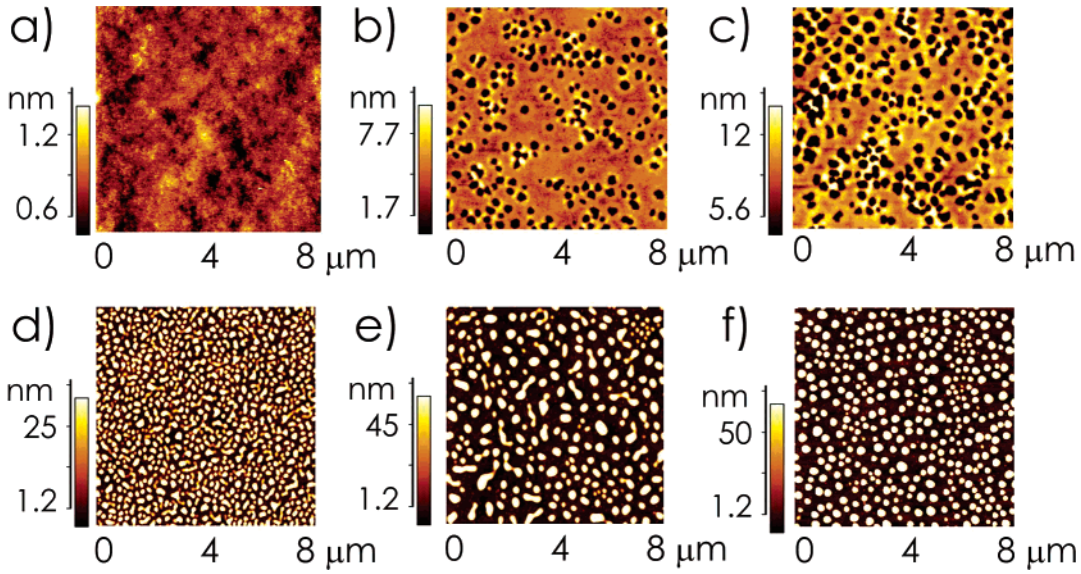

Figure 3. AFM micrographs picturing the surface topography after (a) 0, (b) 10, (c) 20, (d) 45, (e) 90, and (f) 180 min heating at 130 °C for the samples treated by wiping. Each measurement covers a scan range of 8 μm × 8 μm. The height scale is adjusted to emphasize on the characteristic surface features.

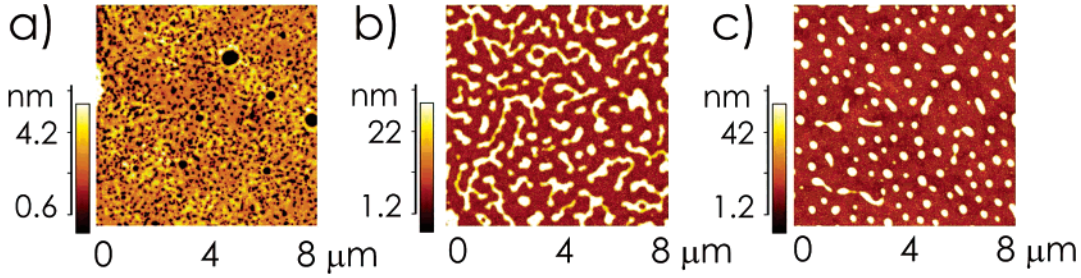

Figure 4. AFM micrographs picturing the surface topography after (a) 90, (b) 240, and (c) 360 min heating at 130 °C for the samples treated by Milli-Q storage. Each measurement covers a scan range of 8 μm × 8 μm. The height scale is adjusted to emphasize on the characteristic surface features.

onto the substrate, which is started to spin. During the initial stage most of the solution is cast off, leaving a thin layer on the substrate. As the layer thins due to fluid flow, the evaporation of the solvent becomes important. The evaporation increases the viscosity of the PS solution and slows the shear thinning of the film. Solvent evaporation freezes in the developing surface structure. According to this three-step model, with the boundary condition of a fixed PS concentration in the toluene solution, the surface cleaning affects the amount of solution flown off during the second step. As a consequence, the slightly deviating final PS film thickness after spin-coating can be understood as a first indication of a changed flow behavior introduced by the cleaning procedures. Moreover, the oxide layer is affected as well by the surface treatments. As compared to the changes in the PS layer thickness, the effect is smaller, but well outside the experimental error bars. The acid and base clean results in slightly thicker oxide layers. In general, the oxide layers are approximately one-fourth in thickness of the PS layers. Although the modification of the oxide layers is very small, it changes the interface potential which rules the behavior of confined PS films.[21]

To prove homogeneity of the PS films right after preparation and probe possible lateral structures introduced by spin-coating, all samples were examined with AFM and GISAXS. In Figures 3 and 5, on the particular example of the cleaning procedure based on wiping, GISAXS and AFM data are presented. The as-prepared status of the samples is denoted with 0 min annealing time. The AFM shows a typical polymer surface with a small statistical surface roughness and no marked surface structures. This is proven by the statistical analysis via Fourier transformation shown in Figure 5. In good agreement with the GISAXS data, the intensity decays with increasing wave vector component q_y, and no peak or shoulder in the intensity is detected beyond the resolution limit.

Evolving Structures. Motion of the liquefied PS is achieved by annealing at 130 °C. Because mass transport predominantly occurs parallel to the sample surface, AFM and GISAXS are very appropriate techniques to monitor the changes. The time-dependent evolution of the topography for each cleaning series is probed with AFM. Figure 5 shows the corresponding AFM micrographs measured at samples pretreated by wiping.

As routinely observed in the case of thicker PS films, the initially continuous film is destroyed by the appearance of holes, growing in time, connected via channels forming islands and finally spherical droplets. The morphological transitions require movement of the polymer chains near the substrate surface due to the small film thickness under investigation. After Fourier transformation, the master curves calculated from the AFM data are compared with the GISAXS data (see Figure 3). A good agreement is obtained between master curves and GISAXS. Therefore, statistically relevant structure information results from the comparison of the length scales with the AFM pictures. This allows for identifying the most prominent in-plane lengths as listed in Table 2 with real-space structures. The dominant length scales are related with diameters of holes and distances between holes at the beginning of the mass transport, followed by the size of islands and distances between neighboring ones and finally correspond to drop diameters and distances.

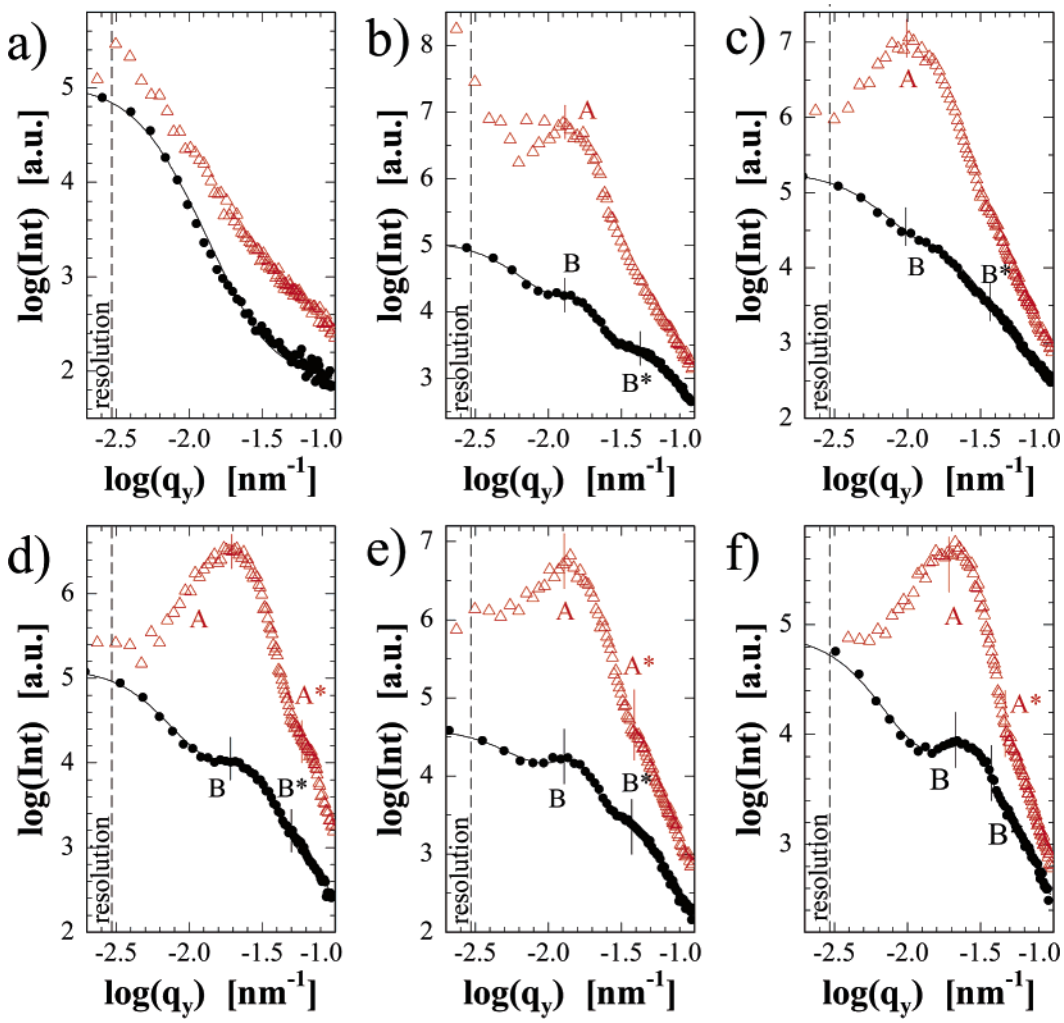

Figure 5. PSD master curves calculated from AFM pictures (red triangles) shown in comparison with horizontal line cuts at the critical angle of PS from the 2D GISAXS measurements (black circles): In the chosen example the Si was treated by wiping. The shown annealing times are (a) 0, (b) 10, (c) 20, (d) 45, and (e) 90, and (f) 180 min at 130 °C. The dominant length scales are marked with A, A*, B, and B* for the PSD curves and GISAXS cuts, respectively. The resolution limit of the scattering experiment is shown with the dashed line.

Table 2. Extracted Dominant Length Scales As Shown in Figure 5 for the Example of Applied Wiping after Different Annealing Times *t*[a]

t [min]	*A* [nm]	*A** [nm]	*B* [nm]	*B** [nm]
0				
10	480 ± 40		487 ± 50	147 ± 25
20	322 ± 32		320 ± 25	125 ± 20
45	634 ± 45	107 ± 20	643 ± 29	125 ± 20
90	490 ± 40	162 ± 20	487 ± 30	169 ± 15
180	326 ± 30	134 ± 20	296 ± 25	165 ± 20

[a] *A* and *A** are dominant length scales belonging to the PSD master curves, and *B* and *B** are dominant length scales of the GISAXS data, respectively. *A* and *B* resemble the distance between holes, islands, and drops; *A** and *B** resemble the diameter of holes, the island, and drop size. Blank fields indicate the absence of any dominant length within the experimental resolution.

Irrespective of the applied surface cleaning, by heating a typical dewetting scenario arises. However, the surface topographies, as observed by AFM, depend on the type of surface treatment (denoted acid, base, Milli-Q, and wiping). Within this scenario, mass is transported differently, depending on the boundary conditions installed by the treatment. Comparing samples treated by wiping with samples treated by Milli-Q, the destabilization process is slowed down, already indicating an altered kinetic. Figure 4 shows three typical stages observable after Milli-Q treatment. Again, the initially homogeneous film is destabilized by dewetting, but retarded as compared to the wiping case (compare for example 90 min of annealing which causes a decay into droplets for the wiped sample (Figure 3e) but only first holes in the case of the Milli-Q stored sample (Figure 4a)).

In contrast, the acid- and base-cleaned samples remain in the state of isolated holes in an elsewhere continuous PS film even after more than hundreds of hours of annealing. The drastic differences are best compared by looking at final or late states as shown in Figure 6 in comparison with Figures 3f and 4c. Drops have formed in the case of a pretreatment with wiping and Milli-Q storage, whereas in both the other cleanings only holes are present. The holes in the acid-treated sample show a bimodal size distribution of holes, whereas the holes in the base-treated sample are extremely small in size at all.

Thus, with respect to stability and dewetting the applied surface cleaning has a strong impact as was already observed in the case of thicker PS films.[13] Taking into consideration the fact that our film thickness is as big as the radius of gyration, it is to be expected that due to the increased contact with the wall the influence of the substrate is enhanced.

With respect to stability, Müller and co-workers[21] calculated the influence of the wall in terms of oxide layer thickness. Along this line, we have to consider the impact of the surface cleaning on the oxide. As probed with X-ray reflectivity the oxide layer

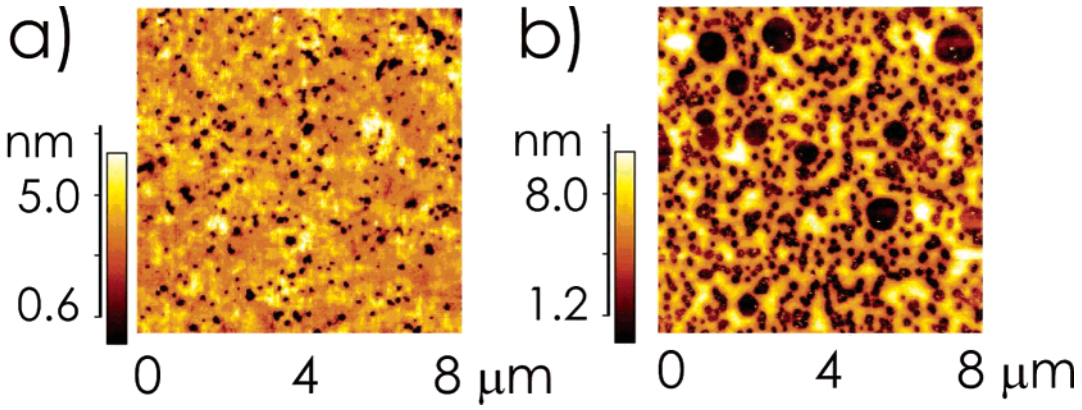

Figure 6. AFM micrographs showing the final states of two of the four different applied Si surface treatments: (a) base and (b) acid. Holes have formed in the case of base and acid clean after 645 h of annealing. Each measurement covers a scan range of 8 μm × 8 μm. The height scale is adjusted to emphasize on the characteristic surface features.

thickness is affected with applying different surface treatments. A comparison to our data fits the obtained results when taking into account, besides the spinodal dewetting, a possible additional binodal dewetting by nucleation. Both cleanings, the acid and the base one, minimize nucleation sites. Thus, nucleation is suppressed, and the slower spinodal destabilization becomes observable for the acid- and base-cleaned samples. Because of the difference in the thickness of the oxide layer (d_{Ox}(acid) > d_{Ox}(base) > d_{Ox}(Milli-Q, wiping), see Table 1) the base cleaning leads to lesser driving force for dewetting at small polymer film thicknesses as compared to the acid cleaning. As a consequence, the PS films on the base treated surfaces exhibit the smallest tendency to dewet from the oxide surfaces, and the smallest holes are observed (see Figure 6a). Following these arguments, the bimodal size distribution of holes observed for the acid treated samples might indicate dewetting due to a spinodal and binodal process. The big holes had formed at impurities and the small holes due to instability. Consequently, the number density of impurities after acid cleaning is larger than after base cleaning, which is in good agreement with previous observations (dewetting of 30 nm thick PS films[13]).

Both the wiping and Milli-Q storage with even smaller oxide layer thicknesses result in again lower energies, but due to the presence of nucleation sites the spinodal process is not relevant. Since polydimethylsiloxane (PDMS) grains have been deposited by the wiping treatment,[13] binodal dewetting is the leading mechanism for these series. The Milli-Q samples show a slower behavior due to the fact that grains were not deposited on purpose but result rather accidentally by the unsophisticated way of storage.

Flow in Confinement. To focus on the kinetics and thereby on the flow of polymer material, the time-dependent evolution is investigated. As shown in Figure 3, the changes on the lateral scale are larger by 3 orders of magnitude as compared to changes in height. Thus, transport of material mainly occurs parallel to the substrate surface. The transformation of covered into uncovered oxide surface is therefore an appropriate measure for flow. Instead of following the growth of isolated holes or drops individually,[39,40] the full changes in the morphology are taken into account by probing the complete dewetted surface area. As a consequence, the experimental errors are reduced and more statistical significant information is obtained. A comparison of the different time scales of the mass transport is shown in Figure 7. It exhibits the free area, not covered with PS, in a double-logarithmic presentation as a function of the annealing time. The error bars capture differences between nominally identical samples as well as experimental errors.

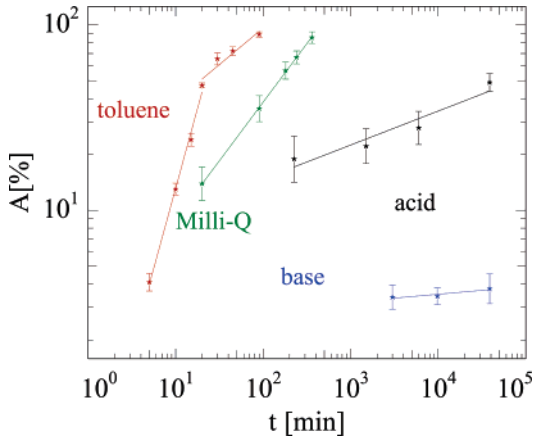

Figure 7. Double-logarithmic plot of the free area not covered with PS in percent vs the annealing time for the four sample series. The solid lines are linear fits to the data points (see Table 3).

Table 3. Slopes Resulting from the Linear Fits to the Double-Logarithmic Data Shown in Figure 7 As Measured at Samples after Different Si Surface Treatment, Denoted with Base, Acid, Milli-Q, and Wiping (Only the First Part)

treatment	slope [log (%)/log [min]]
wiping	1.72 ± 0.09
Milli-Q	0.63 ± 0.01
acid	0.18 ± 0.04
base	0.04 ± 0.02

To every set of data points belonging to one series, a power-law fit is performed. Differences in velocity are well developed. A slowing down from the samples cleaned by wiping to the Milli-Q-pretreated ones to the acid- and base-cleaned samples is depicted. The results of the linear fits are comprised in Table 3. All determined slopes do not match the usual simple slip or no-slip model with $A \sim t^2$ for zero velocity at the substrate and $A \sim t^{4/3}$ for a finite velocity at the substrate−liquid interface. The latter is characterized by its extrapolation to zero velocity at a distance b, the slip length, from the liquid−solid interface in the substrate. Such a behavior was reported for very thick films.[41] In the case of thinner PS films with thicknesses between 30 and 60 nm, destabilized by nucleation, an interpolated behavior between the two limiting cases of perfect sticking (purely viscous dissipation) and full slippage of the film on the substrate was reported.[42] Along this line, the observed slope of the samples which were pretreated by wiping matches to the behavior of partial slippage. The change in slope is due to the different dynamics of hole growth and drop formation. Impurities introduced by the deposition of PDMS grains lead to a

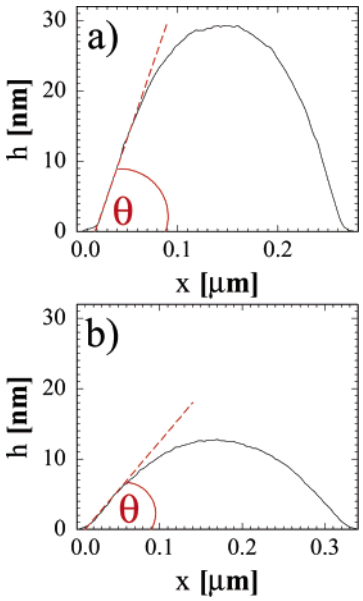

Figure 8. Representative line scans taken from AFM pictures of the samples exhibiting droplets. The applied treatment was (a) wiping and (b) Milli-Q storage. The contact angle, neglecting the small foot part, is indicated.

binodal transport scenario which is still valid in the case of confinement. The friction of the PS molecules at the oxide surface is finite such that there is a certain amount of slippage.

However, the three other series do not match with the kinetics of a partial slippage, and mass transport occurs significantly retarded. Because in the confinement regime the contacts of the chains with the underlying oxide are enhanced and movement is strongly forced to be two-dimensional, the boundary condition becomes dominant. Conformational properties of polymer melts confined between two hard walls without structure, as investigated by Monte Carlo simulation of the bond fluctuation model, deviate significantly in the case of confined films.[43] The parallel and perpendicular components of chain extension, bond−bond correlation function, and the structure factor are affected by the presence of the wall. These structural modifications might cause strong changes in the mass transport as well. Moreover, the actual surface chemistry will result in different possibilities to create hydrogen bonds. Within the acid clean the number of H-terminations related to the dominating total number of OH-terminations is increased as compared to the base clean. This results in an increased possibility of creating hydrogen bonds with the end groups of the polymer chains. Following entropic arguments, close to the surface the number of chain ends is strongly increased. Thus, the presence of an increased number of hydrogen bonds might result in a slowing down of the movement, as observed in the experiments.

Late States. As an outcome of the modified kinetic, the late states differ as well. To elaborate the chemical surface modification in terms of surface energies, the contact angles of the structures in the late states are analyzed. Because samples treated with the acid and the base cleaning do not decay into droplets within a reasonable investigation time (see Figure 6: 645 h annealing results in isolated holes only), we restrict this analysis to the two treatments based on wiping and Milli-Q storage. Representative line scans from the AFM data are comprised in Figure 8. Wiping results in higher drops with a larger contact angle of 22.6 ± 2.9° as compared to Milli-Q storage (contact angle 8.3 ± 0.8°). This larger contact angle is in good agreement with the tendency to exhibit a fast destabilization.

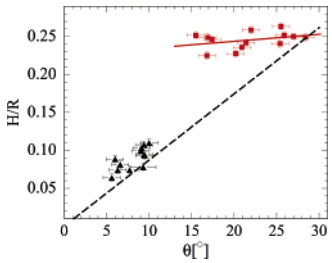

Figure 9. Ratio of height H to radius R as a function of the contact angle in the case of the Milli-Q-treated (triangles) and the wiped (squares) Si samples. The theoretical prediction for systems, which exhibit no influence of the substrate, is shown by the dashed line.

From dewetting of a 5.0 nm PS on thermally oxidized Si (h = 191 nm) a contact angle of 7.5° is reported,[23] whereas on octadecyltrichlorsilane (OTS) covered Si a significantly larger angle of about 58° occurs. Along this line, the larger angle probed in the series pretreated with wiping can be fully attributed to the presence of PDMS on the oxide surface. Despite the big differences in the oxide layer thickness as compared to our investigation, in ref 23 low molecular weight PS has been used, and thus no confinement has been introduced. However, the slightly larger contact angle in the series pretreated with Milli-Q storage might not be due to confinement but rather to the presence of impurities introduced by the cleaning procedure.

In equilibrium, the polymeric drop is given by a full sphere out of which a section is cut by the solid substrate underneath the drop, yielding a spherical cap described by Young's equation $\gamma_{lv} \cos \theta = \gamma_{sv} - \gamma_{sl}$.[44] The assumption of a cylindrical symmetry of the drop is expressed in the radial dependence of the drop height. Within the assumption of a chemical potential difference between bulk liquid and vapor phase $\Delta\mu \rightarrow 0$, the drop profile can be solved analytically. If the influence of the substrate can be neglected the relation between drop height H and drop radius R with $H/R = \theta/2$ should be fulfilled, neglecting corrections of order θ^3. Making use of slight changes in the initial film thickness, we analyzed the resulting final states in terms of the ratio of height H and radius R for several drops as a function of the contact angle θ. The data plotted in Figure 9 for the wiping and the storage treatment are well separated due to the different contact angles. The data of the samples treated with Milli-Q storage are only slightly above the theoretical model pictured by the dashed line. In contrast, the data of the wiped samples deviate from this simple model. Although experimental errors are larger due to the analysis of a limited number of isolated droplets, the deviation from the simple model is obvious. Because PS films without the imposition of confinement have been shown to obey the simple model,[23] the deviations have to be attributed to the presence of the type of boundary. Whereas a less confined system results in a negligible influence of the wall, in confined films the wall chemistry has to be taken into account.

Summary

We investigate the material transport of PS on differently cleaned samples with polymer film thicknesses in the range of the radius of gyration, leading to a confined system in strong contact with the substrate. A well-defined material system (Si, PS) is used together with an established preparation process (spin-coating). The slight differences introduced by different simple cleaning processes of the Si (base and acid bath, Milli-Q storage, and wiping) lead to big changes in the time scales of the observed kinetics. These differences have been addressed by mobilizing the polymer with annealing above the glass

CDV

transition temperature. While a typical dewetting process is observed for the wiping and the Milli-Q storage case, the base- and acid-cleaned samples exhibit only isolated holes in the continuous PS films. Differences in the surface energies are manifested by different contact angles.

Investigation of the surface area not covered by PS allows for detecting the two-dimensional mass transport. PS on the wiped oxide surfaces exhibits a partial slippage, whereas the other treatments result in a general slowing down with respect to the usual slip and no slip condition due to the confinement of the polymer in the thin film.

The different cleaning procedures modify the oxide layer covering the Si substrates as measured by X-ray reflectivity. Although the oxide layer thickness is only slightly changed, the wall potential is affected by these changes. The increase of the oxide layer thickness favors the development of a minimum in the energy density at small film thicknesses leading to a decay of the initially continuous film. For the fastest processes with the smallest oxide layer thickness spinodal decomposition is not energetically favorable, but a binodal mechanism induced by grains dominates the stability. To conclude, in the confined regime small changes of the short-ranged part of the interaction, e.g., by a varying oxide layer thickness, lead to important changes in the kinetics as well as final states. The simple long-ranged part of the interaction is no longer sufficient to fully predict the behavior. As a consequence, scaling down of microfluidic devices will drastically enhance the sensitivity of flow to the detailed structure of the substrate upon which flow is forced. Unexpected results in the flow behavior might result from variations in the substrates chemistry.

Acknowledgment. We thank M. Dommach and R. Döhrmann for their assistance with setting up the GISAXS experiment and S. Valloppilly for his help with the X-ray reflectivity experiments. The used silicon substrates were kindly provided by Wacker Siltronic, Burghausen (Germany). This work was financially supported by the DFG Schwerpunktprogramm SPP 1164 “Nano- and Microfluidics” (Mu1487/2) and within the HASYLAB project II-03-025.

References and Notes

(1) Delamarche, E.; Bernard, H.; Schmid, H.; Michel, B.; Biebuyck, H. *Science* **1997**, *276*, 779.
(2) Weigl, B. H.; Yager, P. *Science* **1999**, *283*, 346.
(3) Ismagilov, R. F.; Ng, J. M. K.; Kenis, P. J. A.; Whitesides, G. M. *Anal. Chem.* **2001**, *73*, 5207.
(4) Thorsen, T.; Maerkl, S. J.; Quake, S. R. *Science* **2002**, *298*, 580.
(5) Dittrich, P. S.; Schwille, P. *Anal. Chem.* **2003**, *75*, 5767.
(6) Unger, M. A.; Chou, H.-P.; Thorsen, T.; Scherer, A.; Quake, S. R. *Science* **2000**, *288*, 113.
(7) Cao, H.; Tegenfeldt, J. O.; Austin, R. H.; Chou, S. Y. *Appl. Phys. Lett.* **2002**, *81*, 3058.
(8) Strook, A. D.; Dertinger, S. K. W.; Ajdari, A.; Mesic, I.; Stone, H. A.; Whitesides, G. M. *Science* **2002**, *295*, 647.
(9) Tice, J. D.; Song, H.; Lyon, A. D.; Ismagilov, R. F. *Langmuir* **2003**, *19*, 9127.
(10) Belder, D. *Angew. Chem., Int. Ed.* **2005**, *44*, 3521.
(11) Müller-Buschbaum, P. *Anal. Bioanal. Chem.* **2003**, *376*, 3.
(12) Müller-Buschbaum, P.; Bauer, E.; Pfister, S.; Roth, S. V.; Burghammer, M.; Riekel, C.; David, C.; Thiele, U. *Europhys. Lett.* **2006**, *73*, 35.
(13) Müller-Buschbaum, P. *Eur. Phys. J. E* **2003**, *12*, 443.
(14) Müller-Buschbaum, P. *J. Phys.: Condens. Matter* **2003**, *15*, R1549.
(15) Reiter, G. *Phys. Rev. Lett.* **1992**, *68*, 75.
(16) Herminghaus, S.; Jacobs, K.; Seemann, R. *Eur. Phys. J. E* **2001**, *5*, 531.
(17) Schäffer, E.; Harkema, S.; Roerdink, M.; Blossey, R.; Steiner, U. *Macromolecules* **2003**, *36*, 1645.
(18) Morariu, M. D.; Schäffer, E.; Steiner, U. *Phys. Rev. Lett.* **2005**, *92*, 156102.
(19) Karapanagiotis, I.; Gerberich, W. W. *Surf. Sci.* **2005**, *594*, 192.
(20) Shin, K.; Hu, X.; Rafailovich, M.; Sokolov, I.; Zaitsev, V.; Schwarz, S. A. *Macromolecules* **2001**, *14*, 4993.
(21) Müller, M.; MacDowell, L. G.; Müller-Buschbaum, P.; Wunnicke, O.; Stamm, M. *J. Chem. Phys.* **2001**, *115*, 9960.
(22) Xie, R.; Karim, A.; Douglas, J. F.; Han, C. C.; Weiss, R. A. *Phys. Rev. Lett.* **1998**, *81*, 1251.
(23) Seemann, R.; Herminghaus, S.; Jacobs, K. *J. Phys.: Condens. Matter* **2001**, *13*, 4925.
(24) Rehse, N.; Wang, C.; Hund, M.; Geoghegan, M.; Magerle, R.; Krausch, G. *Eur. Phys. J. E* **2001**, *4*, 69.
(25) Reiter, G.; Sferrazza, M.; Damman, P. *Eur. Phys. J. E* **2003**, *12*, 133.
(26) Gutmann, J. S.; Müller-Buschbaum, P.; Stamm, M. *Faraday Discuss.* **1999**, *112*, 285.
(27) Müller-Buschbaum, P.; Gutmann, J. S.; Stamm, M. *Macromolecules* **2000**, *33*, 4886.
(28) Parrat, L. G. *Phys. Rev. B* **1954**, *95*, 359.
(29) Salditt, T.; Metzger, T. H.; Peisl, J.; Goerigk, G. *J. Phys. D: Appl. Phys.* **1995**, *28*, A236.
(30) Salditt, T.; Metzger, T. H.; Peisl, J.; Reinker, B.; Moske, M.; Samwer, K. *Europhys. Lett.* **1995**, *32*, 331.
(31) Naudon, A.; Babonneau, D.; Thiaudiere, D.; Lequien, S. *Physica B* **2000**, *283*, 69.
(32) Gehrke, R. *Rev. Sci. Instrum.* **1992**, *63*, 455.
(33) Holý, V.; Baumbach, T. *Phys. Rev. B* **1994**, *49*, 10668.
(34) Yoneda, Y. *Phys. Rev.* **1963**, *131*, 2010.
(35) Lawrence, C. J. *Phys. Fluids* **1988**, *31*, 2786.
(36) Schubert D. W. *Polym. Bull. (Berlin)* **1997**, *38*, 177.
(37) Oron, A.; Davis, S. H.; Bankoff, S. G. *Rev. Mod. Phys.* **1997**, *69*, 931.
(38) Spangler, L. L.; Torkelson, M.; Royal, J. S. *Polym. Eng. Sci.* **1990**, *30*, 644.
(39) Lorenz-Haas, C.; Müller-Buschbaum, P.; Kraus, J.; Bucknall, D. G.; Stamm , M. *Appl. Phys. A: Mater. Sci. Process.* **2002**, *74*, S383.
(40) Karapanagiotis, I.; Gerberich, W. W. *J. Appl. Polym. Sci.* **2005**, *98*, 138.
(41) Redon, C.; Brzoska, J. B.; Brochard-Wyart, F. *Macromolecules* **1994**, *27*, 468.
(42) Jacobs, K.; Seemann, R.; Schatz, G.; Herminghaus, S. *Langmuir* **1998**, *14*, 4961.
(43) Cavallo, A.; Müller, M.; Wittmer, J. P.; Johner, A.; Binder, K. *J. Phys.: Condens. Matter* **2005**, *17*, S1697.
(44) Young, T. *Philos. Trans. R. Soc. London* **1805**, *35*, 95.

MA060535Y